nature communications

Article

https://doi.org/10.1038/s41467-024-51694-y

Specific multivalent molecules boost CRISPR-mediated transcriptional activation

Received: 14 January 2024

Accepted: 15 August 2024

Published online: 22 August 2024

Check for updates

Rui Chen[1,2,3,4], Xinyao Shi[1,3], Xiangrui Yao[1,3], Tong Gao[1,3], Guangyu Huang[1,3], Duo Ning[1,3], Zemin Cao[1,3], Youxin Xu[1,3], Weizheng Liang[1,3,5], Simon Zhongyuan Tian[1,2,3], Qionghua Zhu[1,2,3,4], Liang Fang[1,2,3,4], Meizhen Zheng[1,2,3], Yuhui Hu[6,7], Huanhuan Cui[1,2,3,4] ✉ & Wei Chen[1,2,3,4] ✉

CRISPR/Cas-based transcriptional activators can be enhanced by intrinsically disordered regions (IDRs). However, the underlying mechanisms are still debatable. Here, we examine 12 well-known IDRs by fusing them to the dCas9-VP64 activator, of which only seven can augment activation, albeit independently of their phase separation capabilities. Moreover, modular domains (MDs), another class of multivalent molecules, though ineffective in enhancing dCas9-VP64 activity on their own, show substantial enhancement in transcriptional activation when combined with dCas9-VP64-IDR. By varying the number of gRNA binding sites and fusing dCas9-VP64 with different IDRs/MDs, we uncover that optimal, rather than maximal, *cis-trans* cooperativity enables the most robust activation. Finally, targeting promoter-enhancer pairs yields synergistic effects, which can be further amplified via enhancing chromatin interactions. Overall, our study develops a versatile platform for efficient gene activation and sheds important insights into CRIPSR-based transcriptional activators enhanced with multivalent molecules.

Gene transcription is modulated by dynamic interactions between DNA-binding transcription factors (TFs) and *cis*-regulatory elements. TFs consist of DNA-binding domains (DBDs), which possess well-defined protein structures for recognizing specific DNA motifs, and activation domains (ADs) that recruit co-activators and often contain intrinsically disordered regions (IDRs) lacking conventional functional structures[1,2]. The *cis*-regulatory elements recognized by TFs include proximal promoters, where transcription initiation occurs, and distal enhancers, which potentiate transcription via engaging long-range chromatin loops with target promoter mediated by higher-order TF-coactivator complexes[3,4].

To manipulate gene expression and rewire endogenous transcriptional networks, synthetic TFs based on zinc fingers (ZFs)[5,6] and transcriptional activator-like effectors (TALEs)[7–9] have been engineered. More recently, a similar system based on nuclease dead Cas9 (dCas9), terms as "clustered regularly interspaced short palindromic repeat activation (CRISPRa)", has been developed. The first-generation CRISPRa system utilizes a VP64 AD fused with dCas9 to activate the transcription of target gene via guide RNA (gRNA) with sequence complementary to the promoter[10–12]. In order to achieve higher efficiency, subsequent improvements involve modifying either the fused AD or the gRNA design[13,14]. For example, the VPR system fuses VP64,

[1]Shenzhen Key Laboratory of Gene Regulation and Systems Biology, School of Life Sciences, Southern University of Science and Technology, Shenzhen, China. [2]Innovative Center for RNA Therapeutics (ICRT), School of Life Sciences, Southern University of Science and Technology, Shenzhen, China. [3]Department of Systems Biology, School of Life Sciences, Southern University of Science and Technology, Shenzhen, China. [4]Guangming Advanced Research Institute, Southern University of Science and Technology, Shenzhen, China. [5]Central Laboratory, The First Affiliated Hospital of Hebei North University, Zhangjiakou, Hebei, China. [6]Department of Pharmacology, School of Medicine, Southern University of Science and Technology, Shenzhen, China. [7]Joint Laboratory of Guangdong-Hong Kong Universities for Vascular Homeostasis and Diseases, School of Medicine, Southern University of Science and Technology, Shenzhen, China. ✉e-mail: cuihh@sustech.edu.cn; chenw@sustech.edu.cn

p65, and Rta activation domains to dCas9 for synergistic activation[15]. The SunTag system harbors up to 24 GCN4 peptide repeat docking sites on dCas9, thereby recruiting multiple copies of activators via a fused GCN4 antibody to specific genomic loci[16]. The CRISPR/gRNA-directed synergistic activation mediator (SAM) system utilizes modified gRNAs to recruit multiple activation domains via RNA aptamers[17]. All these modifications aim to increase the local concentration of transcriptional activators at target genomic sites. However, these approaches often require multiple bulky fusion partners, potentially hindering delivery, particularly in therapeutic applications[18,19].

Liquid–liquid phase separation (LLPS) is a common physical phenomenon where IDRs or modular domains (MDs) in proteins can drive formation of biomolecular condensates or membraneless organelles, compartmentalizing biochemical reactions[20]. During gene transcription, TFs and their co-activators, often comprising IDRs, modulate the formation of transcriptional condensates through homotypic and/or heterotypic multivalent interactions[21,22]. Transcriptional condensates at super enhancers have been shown to drive the transcription of highly active genes[23]. In addition, fusion of the IDR of FUS protein to TetR-VP16 enabled phase separation and increased transcriptional activation[24]. More recently, IDRs of NUP98 and FUS were also reported to enhance the transcriptional activation potential of dCas9-VPR[25]. However, two recent studies proposed that optimized multivalent interactions, rather than LLPS per se, enhance transcriptional activation[26,27]. Moreover, Chong et al. found that while IDRs that augment multivalent scaffolding robustly amplify gene expression, excessive LLPS can inhibit transcription[26]. Though the intricate role of LLPS in transcriptional regulation remains controversial, harnessing multivalent interactions hold a promise for the further development of enhanced transcriptional activation system.

Here, to utilize multivalent interactions for enhancing the potency of CRISPR-based transcriptional activation, we screen a panel of 12 IDRs. Although all these IDRs are well-known for their capability to induce phase separation, only seven can augment activation. Using dCas9-VP64-FUS as an example, we demonstrate that cells, both with and without dCas9 microscopic foci formed by phase separation, show potent transcriptional activation of the target gene. In addition to IDR, we investigate several MDs, another class of molecules facilitating multivalent interactions, but not yet associated with transcriptional regulation. Interestingly, while MDs alone do not enhance dCas9-VP64 activity, their fusion with dCas9-VP64-IDR results in substantial further enhancement of transcriptional activation. Furthermore, by varying the number of gRNA binding sites and fusing dCas9-VP64 with IDRs and MDs of different multivalent capabilities, we uncover that optimal, rather than maximal, *cis–trans* cooperativity is crucial for robust activation. Finally, by simultaneously targeting promoter–enhancer pairs, our enhanced activation system shows synergistic effects, which are critically dependent on IDRs and further amplifiable via enhancing chromatin interactions. Thus, our study develops a versatile platform not only for efficient gene activation, but also for studying the underlying molecular mechanisms.

Results

Some but not all IDRs enhance the activation potency of dCas9-VP64

To systematically evaluate the effect of various IDRs, we generated a panel of fusion proteins comprising dCas9-VP64 linked to diverse IDRs (dCas9-VP64-IDR; Fig. 1a). The sources and details of these IDRs are presented in Fig. 1b and Supplementary Data 1. All these IDRs are well-known for their capability to induce phase separation both in vitro and in vivo[28–36]. We then utilized a HEK293T reporter cell line (HEK293R, Fig. 1a) expressing a GFP cassette under control of seven tetracycline operators (7xTetO) plus a minimal CMV promoter[37]. As expected, co-transfection of dCas9-VP64 and guide RNAs targeting the TetO element (gTetO) resulted in moderate activation of GFP (Fig. 1c and Supplementary Fig. 1a). For dCas9-VP64-IDR fusions, we found that some, but not all IDRs enhanced the activation capacity of dCas9-VP64, as demonstrated by increased proportions of GFP-positive cells (Supplementary Fig. 1a) as well as elevated median GFP intensities compared to dCas9-VP64 alone (Fig. 1c). Specifically, IDRs from human FUS, EWS, TAF15, YTHDF1-3, and yeast NUP49 (active IDRs) significantly boosted activation, while IDRs from human CCNT1, TDP43, Tau, hnRNPA2 and rat Erc2 (inactive IDRs) did not improve or even slightly inhibited dCas9-VP64 activity (Fig. 1c). As indicated by the intensity of co-translated BFP (Supplementary Fig. 1b) and the staining of the Flag tag at the N-terminus of dCas9 activators (Supplementary Fig. 1c), the differential activation capabilities of the two IDR groups were not due to their expression levels. Moreover, to verify whether the active IDRs alone could promote gene transcription on their own, we directly fused these IDRs to dCas9 and analyzed their impacts on the activation of GFP expression. As shown in Supplementary Fig. 1d, dCas9-IDR fusions did not induce GFP expression, suggesting that IDRs act as amplifiers rather than direct activators in our system. Finally, to develop a useful tool for modulating gene expression, in addition to the efficiency, it is important to evaluate its specificity or off-target effects. Using dCas9-VP64-FUS as a representative example, we performed mRNA sequencing to assess the transcriptome of HEK293R cells co-expressing dCas9-VP64-FUS with either gTetO or a scrambled gRNA (gScr). As shown in Fig. 1d, e, dCas9-VP64-FUS significantly enhanced GFP expression, with more than 500-fold increase in the gTetO group. More importantly, GFP was the only differentially expressed gene (|Log2 (fold change)|>1, FDR < 0.05), demonstrating that dCas9-VP64-FUS specifically activates target genes with negligible off-target effects.

IDR-enhanced CRISPRa works on endogenous genes

Given that transcriptional regulation of endogenous genes is more intricate than that of the reporter, we proceeded to evaluate the potential of dCas9-VP64-IDR fusion proteins to activate expression of endogenous genes. For this purpose, we designed gRNAs targeting the promoters of four different genes, namely *NTF3*, *ASCL1*, *MYOD1*, and *IL1RN*, and co-transfected them with either dCas9-VP64 or dCas9-VP64-FUS into HEK293T cells. We then measured the expression of these target genes using quantitative reverse transcription PCR (RT-qPCR). As shown in Fig. 2a–d, fusing FUS IDR to dCas9-VP64 significantly enhanced the transcriptional efficiency of these endogenous genes. Moreover, dCas9-VP64-FUS also exhibited superior ability when activating multiple genes using gRNAs targeting promoters of *NTF3*, *ASCL1*, and *MYOD1* simultaneously (Supplementary Fig. 2), demonstrating that our system can be used for multiplex activation of endogenous genes. Furthermore, to evaluate the generalizability of the FUS IDR in CRISPR-based gene activation system, we substituted the Cas protein or AD in the dCas9-VP64-FUS activator. As shown in Fig. 2e–h, by replacing dCas9 with dCpf1 or VP64 with VPR, the FUS IDR significantly boosted the activation ability of both dCas9-VPR and dCpf1-VP64 on endogenous genes.

The multivalent interactions mediated by IDRs are crucial for enhancing transcriptional activation

IDRs can engage in multivalent interactions between the low-complexity sequences. To investigate whether the ability of IDRs to enhance CRISPRa is through such multivalent interactions, we generated a dCas9-VP64-FUS^{27YS} fusion protein where all 27 tyrosine residues in the FUS IDR were mutated to serine, thereby abolishing its ability to form multivalent interactions while preserving intrinsically disordered property[38]. In contrast to the wild-type FUS IDR, the addition of the FUS^{27YS} mutant failed to amplify dCas9-VP64 activation of the GFP reporter (Fig. 3a) as well as endogenous genes (Fig. 3b, c). Furthermore, we divided the FUS IDR into three parts and reshuffled them to generate the activators containing various scrambled FUS sequences,

https://doi.org/10.1038/s41467-024-51694-y

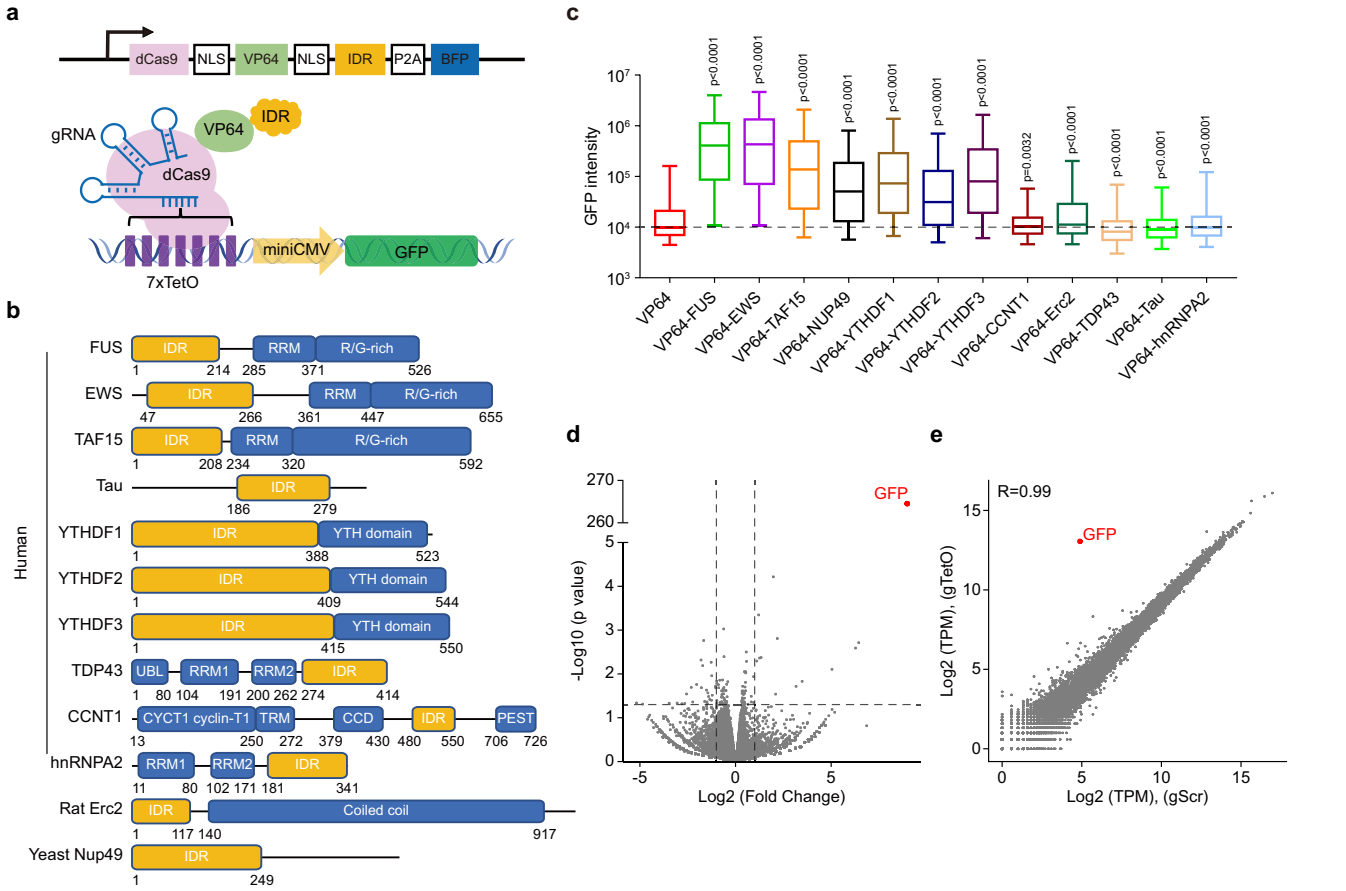

Fig. 1 | dCas9-VP64-IDR robustly activates reporter gene with high specificity. **a** Schematic representation of dCas9-VP64-IDR targeting a Tet-on GFP reporter. The GFP expression in this reporter is regulated by seven tandem tetracycline operator (7xTetO) sequences along with a minimal CMV promoter. Binding of the dCas9-VP64-IDR fusion protein to the TetO sites activates GFP expression. **b** Domain architectures of proteins containing intrinsically disordered regions (IDRs). The specific IDR fragments fused to dCas9-VP64 in this study are highlighted in yellow. **c** Boxplot illustrating the GFP intensity in HEK293R cells expressing dCas9-VP64 or dCas9-VP64-IDR fusions, in combination with a guide RNA targeting the TetO elements (gTetO). The results are presented as the median GFP intensity, along with the 25th and 75th quartiles, as well as the 5th and 95th percentiles, and are representative of three independent experiments. Statistical significance was determined by two-sided Wilcoxon rank-sum test. Cell numbers from left to right (n = 14,983, 13,741, 15,366, 14,226, 18,070, 16,249, 14,173, 12,839, 12,335, 9112, 16,921, 19,733, 12,970). **d** Volcano plot comparing the gene expression profile of HEK293R cells expressing dCas9-VP64-FUS with a gRNA targeting TetO (gTetO) to that with a scrambled gRNA (gScr) control. The x-axis represents the Log2 fold change in gene expression between the two conditions, while the y-axis displays −Log10 p value. Differentially expressed genes were determined using the criteria of |Log2 (fold change)| > 1 and FDR < 0.05, with GFP (marked in red) being the only gene meeting these criteria. Statistical significance was determined by two-sided Wald test with Benjamini–Hochberg correction. **e** Correlation of gene expression profile of HEK293R cells expressing dCas9-VP64-FUS with a gRNA targeting TetO (gTetO) to that with a scrambled gRNA (gScr) control. The x-axis represents the Log2 TPM of control group and y-axis displays the Log2 TPM of activation group. Pearson correlation coefficient (R) = 0.99. The source data for Fig. 1d, e are deposited under accession number GSE248523. Source data are provided as a Source data file.

namely FUS-132, FUS-213, FUS-231, FUS-312, and FUS-321 (Supplementary Fig. 3b). Subsequently, we assessed the activation potential of these activators on the GFP reporter and two endogenous genes. As shown in Supplementary Fig. 3c–e, there was no significant difference in the activation of endogenous genes among these activators. The FUS-321 mutant exhibited a slightly higher activation effect only on the reporter gene compared to the other activators. These results together suggested that both the amino acid composition and the intact multivalent interaction ability are essential for the enhancement effect of FUS IDR.

To check whether IDR-containing dCas9 activators form biomolecular condensates via LLPS, we co-expressed BFP-tagged dCas9-VP64-IDR fusion proteins with a gTetO in the HEK293R cells to visually examine condensate formation and correlate that with transcriptional activation. Active IDR fusions including dCas9-VP64-FUS and dCas9-VP64-YTHDF1 formed multiple distinct puncta and robustly activated GFP expression (Supplementary Fig. 3a). In contrast, the FUS^{27YS} mutant significantly interfered with puncta formation and GFP activation (Supplementary Fig. 3a). Interestingly, inactive IDR fusions such as dCas9-VP64-TDP43 and dCas9-VP64-CCNT1 also generated puncta in cells yet did not enhance GFP expression (Supplementary Fig. 3a). Subsequently, we assessed the fluidity of dCas9-VP64-FUS and dCas9-VP64-TDP43 puncta through fluorescence recovery after photobleaching (FRAP) analysis. As shown in Fig. 3d, dCas9-VP64-FUS displayed rapid fluorescence recovery, while dCas9-VP64-TDP43 showed a relatively slower recovery rate (Fig. 3e). Moreover, we found that visible puncta were present in only around 46% (Supplementary Fig. 3f) dCas9-VP64-FUS expressing cells with a wide range of GFP expression (Supplementary Fig. 3a). The GFP intensity and puncta number as well as the BFP intensity measured in 200 cells also manifested no correlation (Supplementary Fig. 3g, h). Taking together, our analysis suggested that the ability of IDRs to engage in multivalent interactions, rather than that for inducing phase separation per se, governs their capabilities of transcriptional activation enhancement.

Next, if the activation enhancement was via multivalent interaction, the tandem fusion of multiple active IDRs should further increase

https://doi.org/10.1038/s41467-024-51694-y

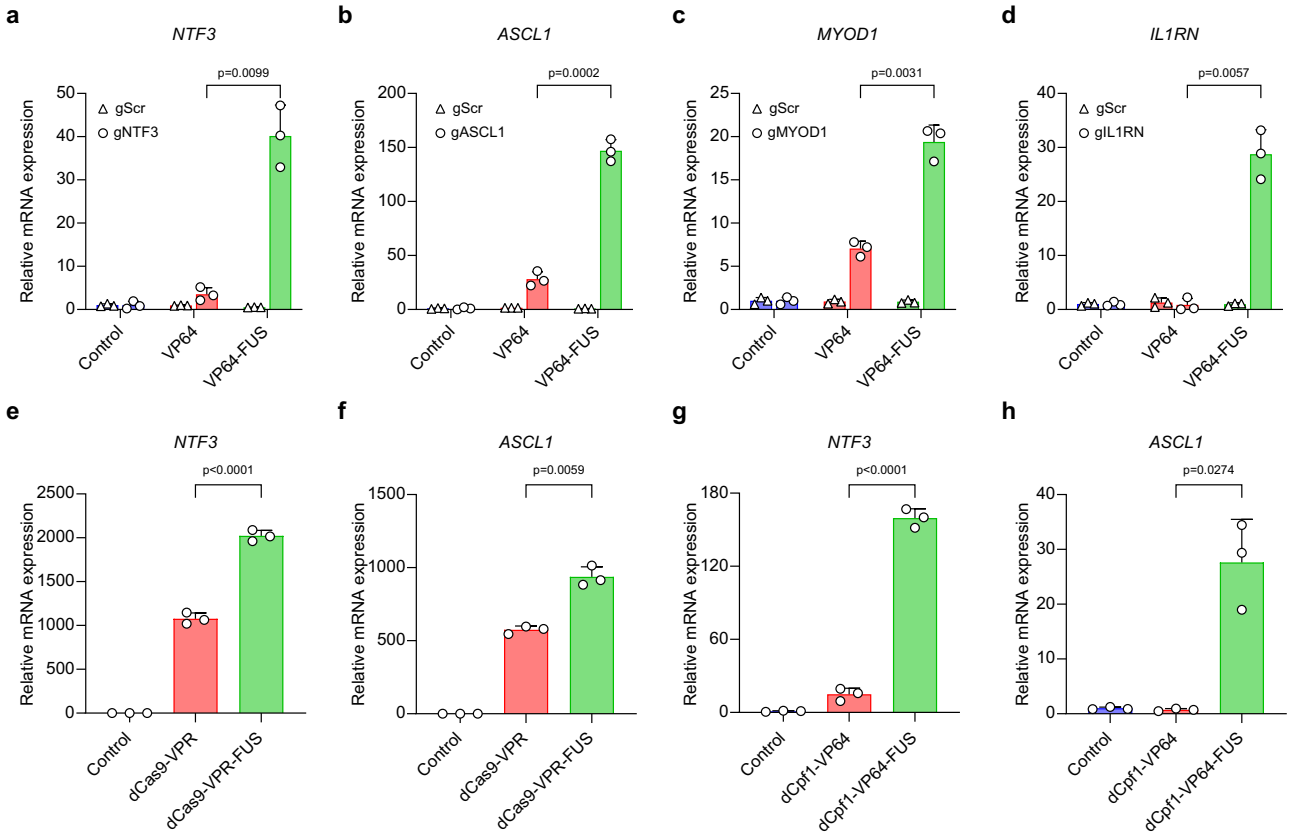

Fig. 2 | Endogenous genes activated by dCas9-VP64-IDR. a–d Relative mRNA expression of *NTF3*, *ASCL1*, *MYOD1*, and *IL1RN* in HEK293T cells transfected with dCas9-VP64 or dCas9-VP64-FUS and a single guide RNA (gRNA) targeting each gene promoter as well as a scrambled gRNA (gScr) control. Data are shown as mean ± SD ($n = 3$ independent experiments). Statistical significance was determined by two-sided Welch's t-test. **e**, **f** Relative mRNA expression of *NTF3* and *ASCL1* in HEK293T cells transfected with dCas9-VPR or dCas9-VPR-FUS and a gRNA targeting each gene promoter. Data are shown as mean ± SD ($n = 3$ independent experiments). Statistical significance was determined by two-sided Welch's t-test. **g**, **h** Relative mRNA expression of *NTF3* and *ASCL1* in HEK293T cells transfected with dCpf1-VP64 or dCpf1-VP64-FUS and a gRNA targeting each gene promoter. Data are shown as mean ± SD ($n = 3$ independent experiments). Statistical significance was determined by two-sided Welch's t-test. Source data are provided as a Source data file.

activation efficiency. To check this, using dCas9-VP64-FUS as an example, we extended the C-terminus with additional IDRs of FUS, EWS, or TAF15. Indeed, the addition of homologous or heterologous IDRs additively enhanced activation of both the GFP reporter (Fig. 3f) and endogenous genes (Fig. 3g, h), suggesting a positive correlation between IDR-mediated multivalent interaction and transcriptional activation.

Finally, to investigate whether IDRs recruit specific transcriptional or chromatin regulatory factors for transcriptional regulation, we performed co-IP analysis and revealed that both the effective dCas9-VP64-FUS and the non-effective dCas9-VP64-TDP43 could interact with BRG1, the core catalytic subunit of the BAF complex, but not the Mediator component MED1 (Fig. 3i). Intriguingly, only dCas9-VP64-FUS showed an interaction with the RNA polymerase II subunit RPB1 (Fig. 3i). Furthermore, to investigate whether these factors could be recruited to the targeted locus, we conducted ChIP-qPCR analysis at the promoters of *NTF3* and *IL1RN*, which were targeted by the respective gRNAs. As shown in Fig. 3j, k, fusion of either effective IDR FUS or non-effective IDR TDP43 to the dCas9-VP64 activator exhibited similar DNA-binding capabilities. Consistent with the co-IP results, BRG1, but not MED1 was notably enriched at these regions when the regions were targeted by both the effective dCas9-VP64-FUS and non-effective dCas9-VP64-TDP43. However, RPB1 enrichment was observed only when the promoters were targeted by dCas9-VP64-FUS, in consistence with the RNA expression data. In addition, we utilized two distinct shRNAs to knock down the expression of BRG1 (Supplementary Fig. 3i). As shown in Supplementary Fig. 3j–l, a significant reduction in the activation efficiency of dCas9-VP64-FUS on both the GFP reporter and endogenous genes was observed (Supplementary Fig. 3j–l), suggesting the necessity of the BAF complex in the activation of target genes. However, as both the effective dCas9-VP64-FUS and the non-effective dCas9-VP64-TDP43 could recruited BRG1 to the targeted locus, the recruitment of BAF complex is not sufficient for transcriptional activation.

IDR and MD cooperatively enhance transcriptional activation

In addition to IDRs, MDs represent another class of protein domains that can self-assemble into higher-order oligomers through multivalent interactions and undergo phase separation. To test whether MDs can enhance activation efficiency, we linked two MDs, the NTD domain of Par3 (Par3 MD)[39] and a simplified Shank3 protein containing the PDZ, HBS, CBS and SAM domains (Shank3 MD)[40], to dCas9-VP64, respectively (Supplementary Data 2). Surprisingly, both MDs failed to enhance the transcriptional activation ability of dCas9-VP64 on the GFP reporter as well as endogenous genes (Fig. 4a, b, Supplementary Fig. 4a).

Inspired by a recent study showing that MD could largely enhance the ability of IDR-induced phase separation in vitro[41], we hypothesized that IDR and MD in combination might further enhance transcriptional activation. Toward this goal, we linked the MDs of Par3 or Shank3 to dCas9-VP64-FUS and observed a much stronger activation efficiency on endogenous genes (Fig. 4a, b). Next, to test whether this enhancement was caused by MD-mediated multivalent interactions, we mutated methionine 1793 in the SAM domain of Shank3 to alanine

https://doi.org/10.1038/s41467-024-51694-y

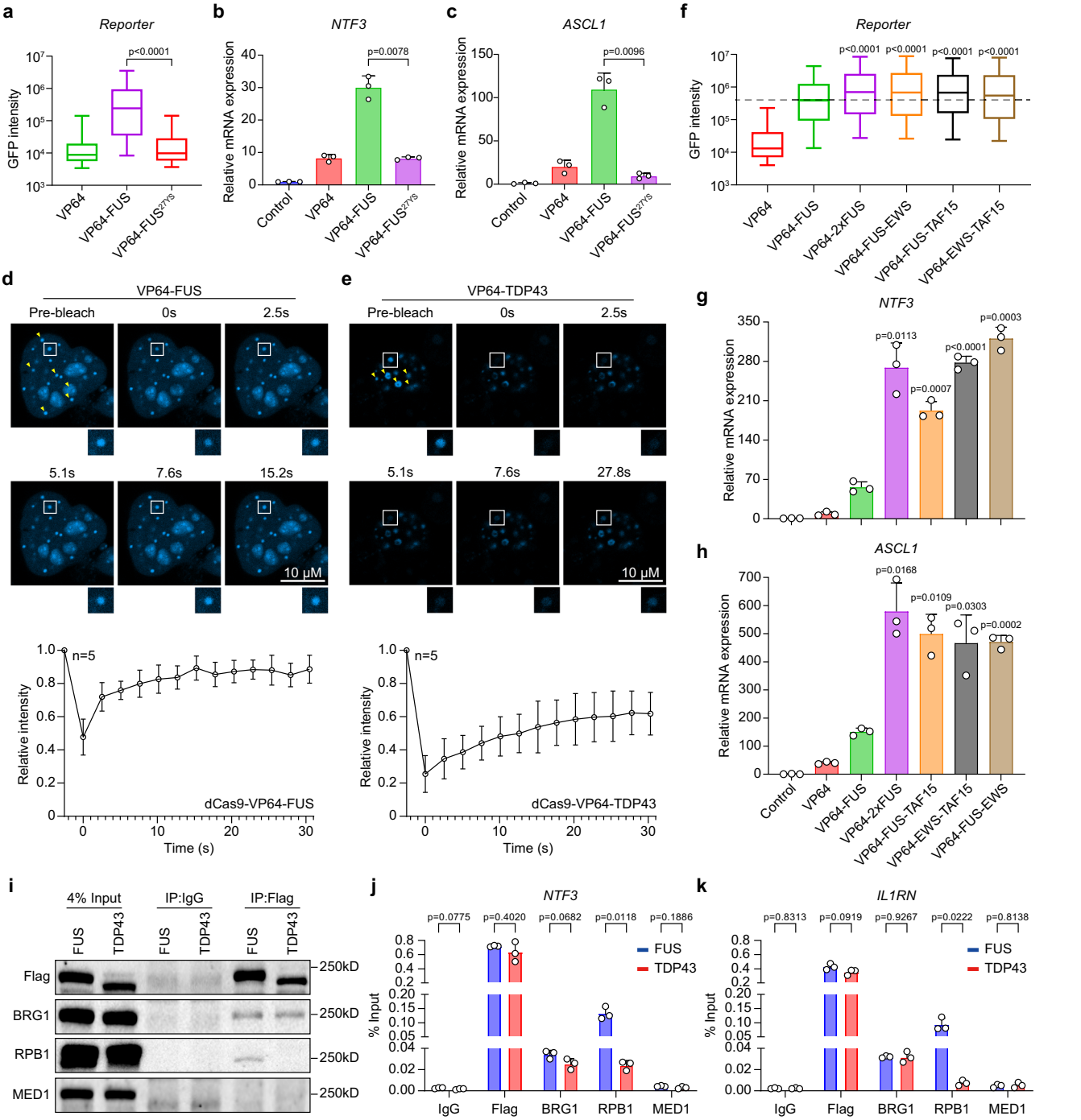

Fig. 3 | IDR-mediated multivalent interactions and transcriptional activation. **a** Boxplot illustrating the GFP intensity in HEK293R cells expressing different dCas9 activators together with gTetO. The results are presented as the median GFP intensity, along with the 25th and 75th quartiles, as well as the 5th and 95th percentiles, and are representative of three independent experiments. Statistical significance was determined by two-sided Wilcoxon rank-sum test. Cell numbers from left to right (n = 17198, 17379, 9902). **b**, **c** Relative mRNA expression of *NTF3* and *ASCL1* in HEK293T cells expressing different dCas9 activators and a single gRNA targeting the indicated genes. Data are shown as mean ± SD (n = 3 independent experiments). Statistical significance was determined by one-way ANOVA versus the dCas9-VP64-FUS group. **d**, **e** Fluorescence recovery after photobleaching (FRAP) analysis of HEK293R cells expressing BFP-tagged dCas9-VP64-FUS or dCas9-VP64-TDP-43 with gTetO. Up, representative timelapse images after photobleaching. Yellow arrowheads indicate bleached condensates. Scale bar, 10 μm. Down: FRAP curves showing mean ± SD fluorescence recovery of condensates (n = 5 puncta per group). **f** Boxplot illustrating the GFP intensity in HEK293R cells expressing different dCas9 activators together with gTetO. The results are presented as the median GFP intensity, along with the 25th and 75th quartiles, as well as the 5th and 95th percentiles, and are representative of three independent experiments. Statistical significance was determined by two-sided Wilcoxon rank-sum test. Cell numbers from left to right (n = 19,096, 16,734, 13,743, 14,080, 12,071, 17,691). **g**, **h** Relative mRNA expression of *NTF3* and *ASCL1* in HEK293T cells expressing different dCas9 activators and a single gRNA targeting the indicated genes. Data are shown as mean ± SD (n = 3 independent experiments). Statistical significance was determined by one-way ANOVA versus the dCas9-VP64-FUS group. **i** Co-immunoprecipitation (co-IP) of Flag-tagged dCas9 activators, BRG1, MED1 or RPB1. Three independent experiments were performed and similar results were obtained. **j**, **k** Enrichment of Flag-tagged dCas9 activators, BRG1, RPB1, and MED1 at the *NTF3* or *IL1RN* promoter. Data are presented as mean values ± SD (n = 3 independent experiments). Statistical significance was determined by two-sided Welch's t-test. Source data are provided as a Source data file.

https://doi.org/10.1038/s41467-024-51694-y

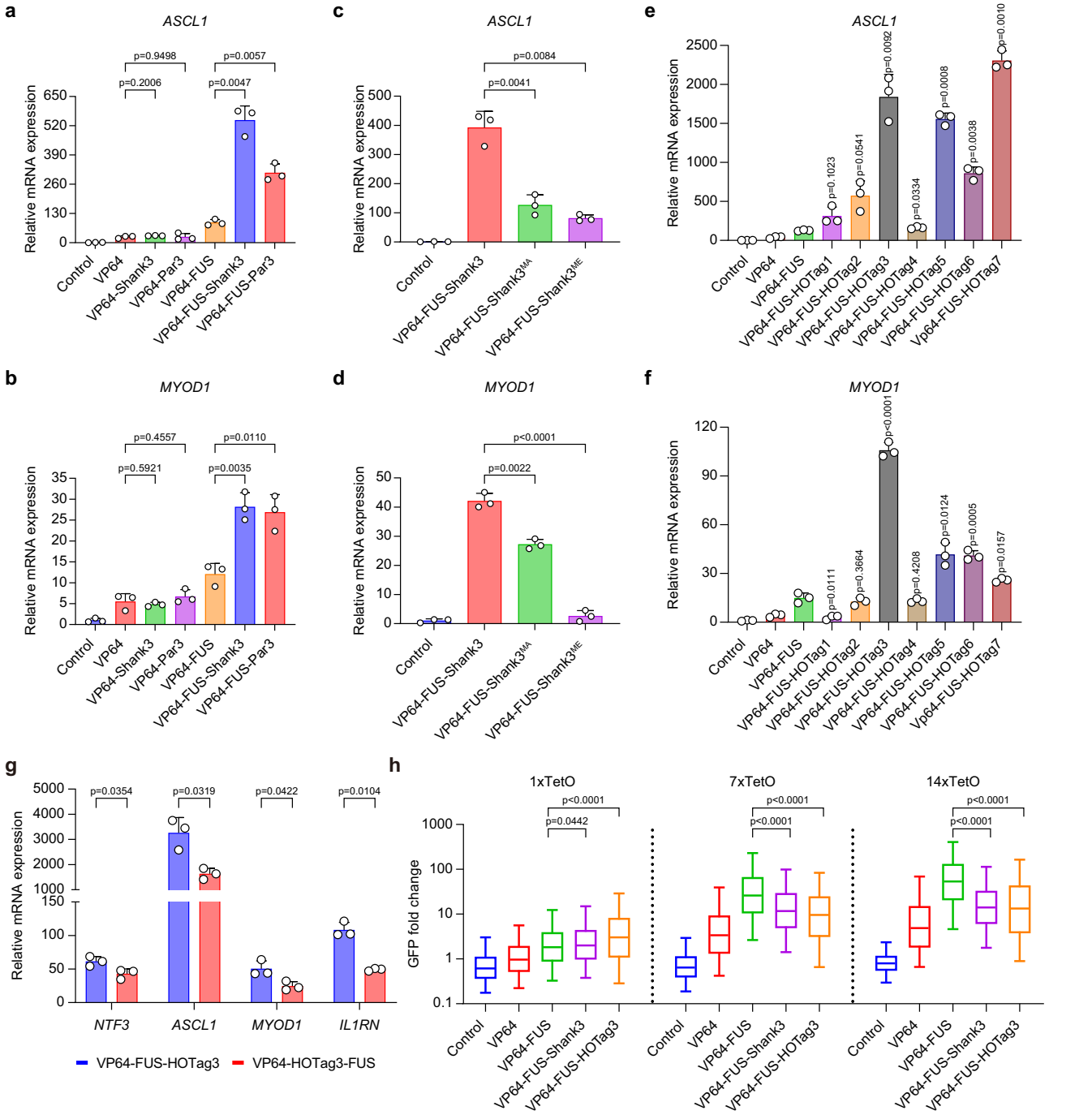

Fig. 4 | Cooperation of IDR and MD in CRISPRa-based transcriptional activation. a, **b** Relative mRNA expression of *ASCL1* and *MYOD1* in HEK293T cells transfected with a single gRNA targeting the indicated genes along with the labeled dCas9-activators. Data are shown as mean ± SD ($n = 3$ independent experiments). Statistical significance was determined by one-way ANOVA versus the dCas9-VP64 or the dCas9-VP64-FUS group. **c**, **d** Relative mRNA expression of *ASCL1* and *MYOD1* in HEK293T cells transfected with dCas9-VP64-FUS-Shank3, dCas9-VP64-FUS-Shank3MA, or dCas9-VP64-FUS-Shank3^{ME} and a single gRNA targeting the indicated genes. Data are shown as mean ± SD ($n = 3$ independent experiments). Statistical significance was determined by one-way ANOVA test versus the dCas9-VP64-FUS-Shank3 group. **e**, **f** Relative mRNA expression of *ASCL1* and *MYOD1* in HEK293T cells transfected with dCas9-VP64-FUS-HOTag activators and a single gRNA targeting the indicated genes. Data are shown as mean ± SD ($n = 3$ independent experiments). Statistical significance was determined by one-way ANOVA test versus the dCas9-VP64-FUS group. **g** Relative mRNA expression of *NTF3*, *ASCL1*, *MYOD1*, and *IL1RN* in HEK293T cells transfected with a single gRNA targeting the indicated genes along with the dCas9-VP64-FUS-HOTag3 or dCas9-VP64-HOTag3-FUS. Data are shown as mean ± SD ($n = 3$ independent experiments). Statistical significance was determined by two-sided Welch's t-test. **h** Boxplot showing relative GFP intensity in 1xTetO-GFP, 7xTetO-GFP or 14xTetO-GFP reporter cells expressing dCas9, dCas9-VP64, dCas9-VP64-FUS, dCas9-VP64-FUS-Shank3 or dCas9-VP64-FUS-HOTag3 together with gTetO. The results are presented as the relative median GFP intensity, along with the 25th and 75th quartiles, as well as the 5th and 95th percentiles, and are representative of three independent experiments. Statistical significance was determined by two-sided Wilcoxon rank-sum test. Cell numbers from left to right ($n = 24{,}461$, 17,298, 21,807, 17,611, 11,280, 22,233, 14,347, 16,136, 15,605, 13,372, 23,028, 11,938, 15,760, 15,641, 12,923). Source data are provided as a Source data file.

(Shank3^{MA}) or glutamic acid (Shank3^{ME}). These two mutations have been demonstrated to disrupt oligomerization of Shank3 to different extents[42]. As shown in Supplementary Fig. 4b, indeed, the Shank3^{ME} mutant effectively disrupted the formation of condensates. As predicted, these mutations also abolished the amplification effect to varying degrees in accordance with their attenuated oligomerization propensities (Fig. 4c, d).

Next, to reduce the size and delivery challenge of dCas9-VP64-IDR-MD fusion proteins, we tested seven short synthetic MDs (~30 amino acids), namely HOTag1-7 (Supplementary Data 2), for enhancing dCas9-VP64-FUS activation of endogenous genes. These HOTags are de novo-designed coiled coils, capable of forming tetramer, pentamer, hexamer, and heptamer, respectively[43]. Similar to natural MDs, HOTags exhibited varying abilities to amplify dCas9-VP64-FUS activation capability, with HOTag3 showing the most significant enhancement (Fig. 4e, f). In contrast, direct fusion of HOTags to dCas9-VP64 did not enhance activation of the same endogenous targets or the GFP reporter (Supplementary Fig. 4c–e), consistent with our previous observation for natural MDs. Finally, we checked whether the order of connecting IDR and MD influenced the activation effect. Interestingly, as shown in Fig. 4g, dCas9-VP64-FUS-HOTag3 induced slightly but statistically significantly higher endogenous gene activation compared to dCas9-VP64-HOTag3-FUS, indicating the importance of optimizing the architecture of fusion protein. Together, the cooperative effects between IDRs and MDs allow substantial enhancement of dCas9-VP64 activator on endogenous genes, dependent on the design and arrangement of the components.

Optimal *cis*–*trans* interactions are required for robust transcriptional activation

Whereas fusing the MDs to dCas9-VP64-FUS enhanced activation of endogenous gene targets compared to dCas9-VP64-FUS alone, surprisingly, the addition of the same MDs inhibited dCas9-VP64-FUS activation of a GFP reporter gene under the control of seven tandem TetO repeats (7xTetO) in HEK293R cells (Supplementary Fig. 4f). Considering that the major difference between endogenous genes and the GFP reporter is that the promoter of the reporter contains seven tandem TetO repeats targeted by our gRNA, we hypothesized that the multivalent interactions provided by fused IDR-MDs may exceed the optimal range for activating the 7xTetO GFP reporter. If this is the case, the IDR-MD fusion may still show enhanced activation when the promoter of the reporter gene contains fewer gRNA binding sites. To test this, we compared fusion proteins with or without IDR and MD in parallel on GFP reporters under control of different numbers of gRNA binding sites, namely 1xTetO, 7xTetO, and 14xTetO. As expected, for the same activator, more binding sites always led to higher transcriptional activation. Interestingly, whereas for the 1xTetO reporter, GFP intensity positively correlated with the multivalent capacity of dCas9-based activators, the activator containing IDR-MD with the highest multivalent capacity failed to further enhance GFP expression in the 7xTetO and 14xTetO reporters (Fig. 4h). A similar phenomenon was also observed for dCas9-VP64 fused with 1x, 2x, and 3x FUS IDR (Supplementary Fig. 4g). Collectively, our findings demonstrate that an excess of *cis*–*trans* interactions can lead to a decrease in efficiency of transcriptional activation. This suggests that achieving robust transcriptional activation might require optimal cooperativity between *trans*-acting factors and *cis*-regulatory DNA elements.

Simultaneously targeting enhancer-promoter synergistically boosts gene activation

Enhancers are distal *cis*-regulatory elements that can interact with target gene promoters, bringing bound transcriptional co-activators into proximity to regulate transcription. First, to test our IDR/MD-containing activators in modulating enhancer activity, we chose the well-characterized human β-globin locus, which contains β-like globin genes (*HBB*, *HBD*, *HBE,* and *HBG1/2* as well as a pseudogene *HBBP1*) that are developmentally regulated by a shared upstream enhancer cluster known as the locus control region (LCR) (Fig. 5a). The LCR consists of five DNase I hypersensitive sites (HS1-HS5) among which the HS2 enhancer has been extensively studied as an erythroid-specific enhancer playing a critical role in regulating the transcription of β-globin genes within this locus[44]. As shown in Supplementary Fig. 5a–e, compared to the dCas9-VP64, targeting IDR/MD-containing activators to the HS2 enhancer led to higher though still moderate activation, but only for *HBG1/2*.

Given that enhancer-promoter communication can be mediated by multivalent protein-protein interactions, we investigated whether concurrently guiding the synthetic activators containing multivalent molecules to endogenous enhancer-promoter pairs could synergistically promote target gene activation (Fig. 5b). Indeed, compared to targeting either enhancer or promoter alone, simultaneous targeting of the HS2 enhancer and the promoter of individual β-globin genes by IDR/MD-containing activators led to substantially higher gene activation. As shown in Fig. 5c–g, the expression of all the β-globin genes (*HBE*, *HBG1/2*, *HBD,* and *HBB*) and the pseudogene *HBBP1* could be synergistically boosted by dCas9-VP64-FUS and dCas9-VP64-FUS-HOTag3, whereas no such synergy was observed for dCas9-VP64. Moreover, we designed gRNAs to target the flanking regions of the HS2 enhancer (2–2.5 kb and 0.5–1 kb upstream or downstream of the HS2 region). As shown in Supplementary Fig. 5f, g, compared to the HS2 enhancer, simultaneous targeting its flanking regions and the promoter of β-globin genes by dCas9-VP64-FUS resulted in a notable decrease in activation to varying degrees. The extent of decrease is correlated with the distance from the HS2 enhancer, which demonstrated the specificity of simultaneous targeting of enhance/promoter pair. Furthermore, this synergistic effect was also observed when the enhancer-promoter pair of *MYOD1* was targeted by IDR/MD-containing activators (Supplementary Fig. 5h). Together, our data suggested the superiority of multivalent molecules in activating gene expression by simultaneously targeting enhancer-promoter pairs.

Enhancing chromatin interactions further amplifies transcriptional activation

To test whether enhancing enhancer-promoter interactions could further amplify gene expression, we engineered inducible dimerization of dCas9 and dCpf1 fusions using the ABA-induced ABI1-PYL1 system, which has been demonstrated to modulate chromatin interactions[45]. Specifically, we appended ABI1 and PYL1 dimerization partners to dCas9-VP64-FUS and dCpf1-VP64-FUS, respectively, and then guided them to enhancer or promoter using specific gRNAs (Fig. 6a). For comparison, we also generated several control fusion proteins lacking VP64, FUS IDR, or both. In the absence of ABA, targeting the HS2 enhancer and *HBD* or *HBG1/2* promoter with ABI1-mCherry-dCas9-VP64-FUS and PYL1-BFP-dCpf1-VP64-FUS, respectively, led to higher expression of *HBD* or *HBG1/2*, respectively, confirming synergistic activation by dual targeting as observed above (Supplementary Fig. 6a, b). Strikingly, the addition of ABA to induce ABI1-PYL1 heterodimerization further significantly enhanced the activation of *HBD* and *HBG1/2*, but only when both the enhancer and promoter were targeted by VP64-FUS fusions (Fig. 6b, c, Supplementary Fig. S6c, d), again highlighting the essential contribution of FUS IDR for such synergistic effect. Furthermore, we designed gRNA and crRNA to recruit dCas9-VP64-FUS and dCpf1-VP64-FUS to the enhancer and promoter regions of the human *MYOD1* gene, respectively. As illustrated in Supplementary Fig. 6e, the presence of ABA notably boosted the activation of *MYOD1*.

To further investigate the specificity of enhancer-promoter interactions in our synthetic system, we utilized the same tethering strategy to target the HS2 enhancer and the promoter regions of *UBQLN3* or *TRIM22*, which are not direct targets of HS2. These

https://doi.org/10.1038/s41467-024-51694-y

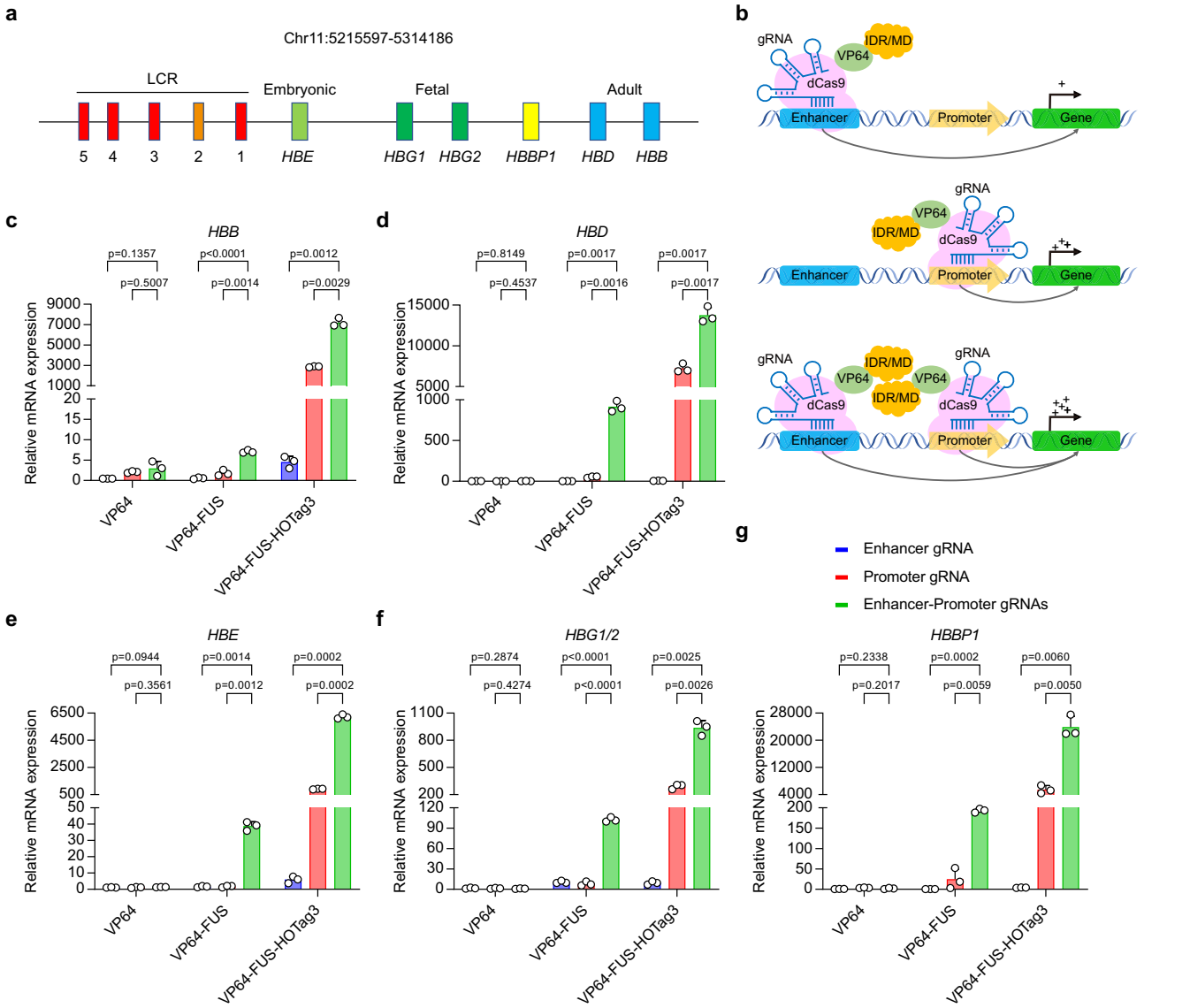

Fig. 5 | Synergistic activation by concurrently targeting enhancer-promoter pairs. a Schematic of the human β-globin locus including Locus Control Region (LCR), downstream *HBB*, *HBD*, *HBG1/2*, *HBE* genes, and *HBBP1* pseudogene. The genes in this locus are regulated by the HS2 enhancer (orange). **b** Schematic of dCas9-VP64-IDR/MD targeting an enhancer, promoter, or enhancer-promoter pair. The dCas9-VP64-IDR/MD fusion protein can be guided by gRNAs to bind to enhancer elements (top), gene promoters (middle), or both (bottom) to modulate transcriptional activation. **c**–**g** Relative mRNA expression of *HBB*, *HBD*, *HBG1/2*, *HBE*, and *HBBP1* in HEK293T cells transfected with dCas9-VP64, dCas9-VP64-FUS, or dCas9-VP64-FUS-HOTag3 with promoter gRNA, enhancer gRNA or pooled enhancer-promoter gRNA pair. Data are shown as mean ± SD ($n = 3$ independent experiments). Statistical significance was determined by one-way ANOVA test versus the gRNAs targeting the enhancer-promoter pair group. Source data are provided as a Source data file.

promoter regions are located approximately 230 kb and 400 kb away from the HS2 enhancer, respectively. As shown in Supplementary Fig. 6f, g, in HEK293T cells stably co-expressing ABI1-mCherry-dCas9-VP64-FUS with gHS2 and PYL1-BFP-dCpf1-VP64-FUS with crUBQLN3 or crTRIM22, we observed only a slight increase of *TRIM22* expression, while there was no statistically significant alteration in *UBQLN3* expression following ABA treatment. Taken together, these empirical findings suggested that the amplified activation via tethering distal and proximal elements would work efficiently only for specific enhancer-promoter pairs.

Discussion

While increasing evidence has suggested regulatory roles of multivalent molecules in diverse cellular processes, their precise quantitative contributions to transcriptional control remained to be fully elucidated[46]. In this study, by engineering synthetic CRISPR activators containing IDR/MD, we delineated their roles in the modulation of transcriptional activation. In our engineered system, we found that the induction of transcriptional activation was strictly dependent on the AD, and multivalent molecules themselves could not directly induce gene transcription. This finding aligns well with other studies showing that the presence of an IDR alone is insufficient to activate reporter or endogenous genes in various synthetic systems[24,25,27]. Instead, IDRs and MDs act as amplifiers to enhance the activation of gene transcription in our system. By fusing IDRs and MDs with different multivalent capabilities to the activators, our tool could achieve different expression levels of a target gene, enabling quantitative analysis of the effect of different gene expression levels across a broad range. Moreover, our synthetic system has a negligible off-target effect, comparable to other published CRISPRa approaches[10,15–17]. These findings support incorporating multivalent molecules as an effective strategy to improve CRISPRa efficiency, without compromising specificity.

https://doi.org/10.1038/s41467-024-51694-y

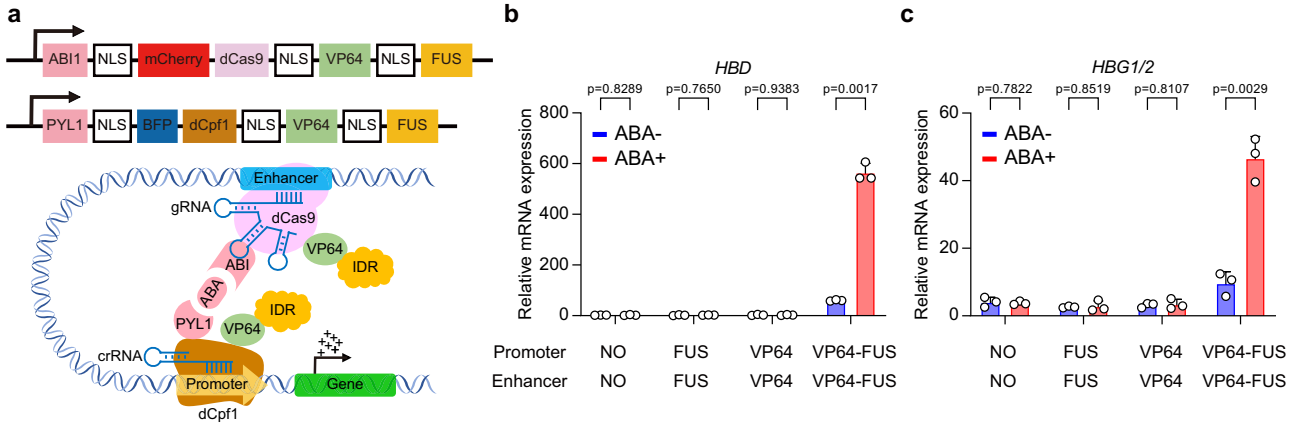

Fig. 6 | Transcriptional activation enhanced via enhancing chromatin interactions. a Schematic of ABI-mCherry-dCas9-VP64-FUS and PYL-BFP-dCpf1-VP64-FUS fusion proteins targeting an enhancer and a promoter, respectively. In the presence of abscisic acid (ABA), ABI1 and PYL1 dimerize, inducing an artificial chromatin loop between the targeted enhancer and promoter regions. **b**, **c** Relative mRNA expression of *HBD* and *HBG1/2* in HEK293T cells expressing ABI1-mCherry-dCas9 fusion proteins targeted to the HS2 enhancer along with PYL1-BFP-dCpf1 fusion proteins targeted to the corresponding gene promoters. Cells were treated with and without abscisic acid (ABA). The effector domains of the enhancer- and promoter-targeted fusion proteins are indicated. Data are shown as mean ± SD ($n = 3$ independent experiments). Statistical significance was determined by two-sided Welch's t-test. Source data are provided as a Source data file.

Although a previous study found that IDRs of FUS and NUP98 could increase the activation capability of dCas9-VPR[25], it remains unclear whether all IDRs hold such potential. Our finding that certain IDRs can enhance dCas9-VP64 activation ability while others cannot, raises an important question: what factors contribute to the specificity of IDRs in boosting gene transcription? While IDRs themselves often exhibit high conformational flexibility[47], it is important to consider physicochemical properties and conformations of IDR fusion proteins within the context of transcriptional activation[48]. However, we observed no significant differences in physicochemical properties between active and inactive IDRs (Supplementary Data 1). Moreover, an IDR's interaction partners can profoundly impact its capacity to amplify gene activation. For instance, FUS IDR interacts with components of the BAF chromatin remodeling complex[49] and engages critical co-activators and chromatin regulators more extensively[50], whereas the IDRs of m6A reader YTHDF proteins may recruit enhancer RNAs to promote gene activation[51]. Our co-IP and ChIP-qPCR data demonstrated that the fusion of either FUS IDR or TDP43 IDR to the dCas9-VP64 activator did not affect its DNA-binding capability, and both fusion proteins could interact with BRG1. However, only the dCas9-VP64-FUS fusion could interact with and recruited the RNA polymerase II subunit RPB1 to the target locus, in consistent with the corresponding RNA expression data. It awaits future study how the differential recruitment of RPB1 was achieved.

IDRs and MDs are two classes of molecules facilitating multivalent interactions and associated with the capacity of forming LLPS. However, MDs differ markedly from IDRs in their amino acid composition and can undergo compact folding[52]. For example, FUS IDR is a well-characterized prion-like domain capable of phase separation by itself[53], while the SAM domain of Shank3 MD can specifically interact with each other in a head-to-tail manner, forming large polymers[42]. IDR interactions are often weak and transient, while MD interactions tend to be relatively strong and more defined[20,54]. Unlike IDRs, the MDs examined in our study did not enhance the activation ability of dCas9-VP64, indicating the role of transient, nonspecific nature of multivalent IDR-IDR interaction in transcriptional activation. However, IDR and MD in combination could cooperatively amplify transcriptional activation. This is likely because the IDR-MD molecule could form a larger but still dynamic molecular network due to the presence of both transient and specific interactions mediated by IDR and MD, respectively. Indeed, it has recently been demonstrated that the IDR-MD chimera of FUS IDR and Shank3 MD can phase separate in vitro at very low concentrations. Interestingly, the Shank3 MD mutants exhibit attenuation of specific interactions for molecular network formation in the condensed phase[41], consistent with our findings on their weak effects on transcriptional activation when combined with FUS IDR. Intriguingly, such synergistic effect of unspecific flexible and specific rigid multivalent interactions on formation of phase separation was often observed in naturally occurring condensates consisting of DNA/TFs or RNA/RNA-binding proteins (RBPs), where IDRs of TFs/RBPs mediate unspecific interactions, whereas DNA/RNA-binding domains facilitate specific interactions with nucleic acids[47,55].

The multivalent ability of synthetic activators is likely the key to enhancing transcriptional activation, where IDRs-mediated multivalent interactions can increase the local concentration of activators and co-activators at target sites, resulting in higher activation efficiency[25,56]. However, we found that visible LLPS-like puncta were not a prerequisite for transcriptional activation, as (1) CRISPR activators containing either active IDRs (FUS, YTHDF1) or inactive IDRs (TDP43, CCNT1) could form LLPS-like puncta and (2) GFP could be activated in reporter cells with and without dCas9-VP64-FUS puncta in our experiments. Therefore, the formation of visible LLPS-like puncta in cells was likely neither required nor sufficient to induce transcriptional activation, in line with a recent publication suggesting that multivalent interactions mediated by IDRs are important for gene activation[27]. However, solely based on current data, we cannot completely exclude the role of forming transcriptional condensates, as some tiny and transient condensates, especially those only at specific transcriptional loci, cannot be observed under the normal confocal microscope.

Previously, Chong et al. found that transcriptional activation requires finely tuned optimal levels of the non-specific interactions mediated by IDRs. Overly high amounts of IDR-IDR interactions can outcompete specific TF-DNA binding, leading to LLPS and transcription repression[26]. Unlike other persistent protein-nucleic acid condensates like the nucleolus and processing bodies, transcriptional activation is a relatively transient and dynamic process, determined by the kinetics of TFs binding to specific DNA sequences[57,58]. By varying the number of gRNA binding sites and applying IDR/MD-containing activators with different multivalent capabilities, we demonstrated that excessive levels of *cis–trans* interactions constrained activation capability, indicating that optimal *cis–trans* cooperativities enable robust transcriptional control. A similar finding was also observed in a recent study using chemically controlled TF clustering to induce gene

transcription[59]. This may also explain the lack of correlation between LLPS-like puncta and GFP expression observed in our imaging experiments. An optimal level of multivalent interactions mediated by IDR-containing activators might be required for efficient activation of the GFP reporter gene. Either too little or too much transcriptional condensates formation could lead to inefficient activation of gene expression. Of course, whether the conclusions from such synthetic systems could be generalized to the regulation of endogenous genes warrants future investigation.

Compared to robust transcriptional activation by targeting promoters, the activation induced by guiding our synthetic activators to enhancers was substantially less efficient, consistent with previous studies using other dCas9-based activators[60–62]. However, by simultaneously targeting enhancer-promoter pairs, we observed a synergistic increase in transcriptional activation. Notably, this synergistic effect was only achieved when employing the dCas9-VP64 activator fused with multivalent molecules, aligning well with emerging evidence that highlights the crucial role of IDR-containing chromatin regulators in organizing long-range chromatin interactions[63,64]. Furthermore, by employing a chemically controlled tethering system to artificially enhance chromatin interactions between the HS2 enhancer and the promoters of two β-globin genes, we could further achieve additional transcriptional enhancement. However, when the same tethering system was applied to the HS2 enhancer and the promoters of *UBQLN3* or *TRIM22*, no efficient activation amplification was observed, likely due to the specificity of enhancer-promoter interactions and the substantial genomic distance between HS2 enhancer and the promoter of *TRIM22* and *UBQLN3*. In the future, our adjustable synthetic system can be employed to systematically dissect the molecular mechanisms underlying productive long-range chromatin interactions in transcriptional control, although the insights gained using the synthetic systems should be extended to endogenous systems always with caveat.

Methods

Cell culture and transfection

The HEK293T cell line was obtained from the American Tissue Collection Center (ATCC, CRL-3216). The HEK293R reporter cells were generously provided by Dr. Zhou Songyang at Sun Yat-sen University[37]. These cells were cultured in DMEM medium with addition of 10% FBS and 1% PS at 37 °C and 5% CO_2. For CRSIPRa transfection, 800 ng of dCas9-fusion protein expression plasmids and 200 ng individual or equimolar pooled gRNA expression plasmids were transfected into cells in 12-well plate by PEI (Sigma, 408727). Following a 24-h culture post-transfection, the transfected cells underwent selection for additional 48 h using puromycin (Yeasen, 60209ES) at a final concentration of 2 μg/μl. Subsequently, these cells were utilized for the following experiments, including flow cytometry, RT-qPCR, and mRNA-seq analyses.

For ABI1-PYL1 inducible double CRSIPRa transfection, 400 ng of PYL1-BFP-dCpf1-based activator, 400 ng of ABI1-mCherry-dCas9-based activator, 100 ng enhancer gRNAs and 100 ng promoter crRNAs expression plasmids were transfected into cells using the same method. After 24 h of culture, puromycin (Yeasen, 60209ES) was added into the medium at a final concentration of 2 μg/μl to select positive cells, while abscisic acid (ABA, MCE, HY-100560) was added at a final concentration of 100 μM to induce the ABI1-PYL1 interaction. Finally, the next experiments were performed three days after transfection.

Plasmids construction

The dCas9-fusion protein expression plasmids were generated by incorporating VP64/VPR, IDRs and/or MDs, P2A-BFP into pB-CAGGS-dCas9 (Addgene, 110823) using Gibson assembly with the Hieff Clone® Universal One Step Cloning Kit (Yeasen, 10922ES). The IDRs and MDs, except synthetic HOTag1-7, were amplified by PCR from human, yeast, or mouse cDNA and the specific details were listed in Supplementary Data 1 and 2. For the dCpf1-VP64-FUS fusion protein expression plasmids, a similar assembly process was followed, with the additional step of replacing dCas9. The synthetic gRNAs or shRNAs, listed in Supplementary Data 3, were inserted into Lenti-guide Puro plasmid (Addgene, 52963) or pLKO.1 puro plasmid (Addgene, 8453), respectively, and expressed under control of a U6 promoter. The 1xTetO-GFP, 7xTetO-GFP, and 14xTetO-GFP reporters were constructed by modifying TetO spacer sequence and replacing APEX2 with GFP in the RAR3-APEX2-FLAG plasmid[65]. To construct the PYL-BFP-dCpf1-VP64-FUS and ABI-mCherry-dCas9-VP64-FUS expression plasmids, the Cas9-P2A-Blast in the lentiCas9-Blast plasmid (Addgene, 52962) was replaced with sequence encoding PYL1/ABI1, BFP/mCherry, and CRISPRa proteins.

Virus package and stable cell line construction

For each virus packaging, HEK293T cells were seeded one day prior and transfected with the lentiviral plasmid, pMD2.G (Addgene, 12259), and psPAX2 (Addgene, 12260), at a ratio of 1.64:0.72:1.3 using PEI (Sigma, 408727). The medium was refreshed 12 h after transfection. After 48 h, the supernatant was collected, followed by centrifugation and filtration through a 0.45-μm filter. The lentivirus particles were concentrated using PEG8000 (Promega, V3011) precipitation and then applied to the targeting cells for transduction.

Flow cytometry analysis

HEK293R cells transfected with dCas9-VP64-IDR/MD and gTetO were dissociated to single-cell suspensions by trypsin. The fluorescence intensities of BFP (excited with 405 nm laser), GFP (excited with 488 nm laser), and mCherry (excited with 561 nm laser) were measured using a flow cytometer (Beckman Coulter, CytoFLEX). To exclude cells without dCas9 fusion expression, only BFP-positive cells were included in the calculation of GFP intensity.

For flow cytometry analysis of Flag-tagged dCas9 activators, transfected cells were dissociated into single-cell suspensions using trypsin. After centrifugation, the cell pellets were fixed and permeabilized with the Transcription Factor Fixation/Permeabilization working solution (Invitrogen, 00-5123 and 00-5223) in the dark for 45 min. Subsequently, the treated cells were washed with Permeabilization Buffer (Invitrogen, 00-8333) and then incubated with an anti-Flag antibody (Proteintech, 20543-1-AP) in the dark for 45 min. Following the removal of unbound antibodies with Permeabilization Buffer, CoraLite594-conjugated secondary antibody was applied to label the Flag-tagged dCas9 activators with 30 min incubation. Finally, the labeled cells underwent two washes with Permeabilization Buffer before being loaded onto a flow cytometer for measurement.

Confocal imaging

HEK293R cells were cultured on a Glass Bottom Cell Culture Dish (biosharp BS-20-GJM) and transfected with dCas9-VP64-IDR fusions with gTetO. After 48 h of transfection, living cell imaging was performed using a Zeiss LSM980 Confocal Microscope. The images were captured using a 63× oil objective with a slice interval of 0.2 μm on the ZEISS ZEN 3.6 Software. The fluorescence proteins BFP and GFP expressed in our cells were excited by 405 nm and 488 nm lasers, respectively. The acquired data was subsequently analyzed using the ZEISS ZEN 3.6 software.

FRAP assay

Fluorescence recovery after photobleaching (FRAP) experiments were conducted using a Zeiss LSM980 Confocal Microscope equipped with a ×63 oil objective. A condensate with a diameter of 0.5–4 μm was selected for analysis. A round region measuring 0.7 μm on each side was chosen for FRAP analysis. The BFP signal was bleached using a 405 nm laser at 100% laser power. Fluorescence intensity changes over

time were recorded for pre-bleaching frames and within 30 s after bleaching. For quantitative analysis, the average intensity of the frames before photobleaching was normalized to 100%. Image analysis was performed using the ZEISS ZEN 3.6 software.

Quantitative reverse transcription-PCR

RNA was extracted from transfected HEK293T cells using the RNA isolater Total RNA Extraction Reagent (Vazyme, R401). Subsequently, cDNA synthesis was performed using the HiScript II Q Select RT SuperMix for qPCR (Vazyme, R233). Real-time PCR was conducted using the ChamQ SYBR qPCR Master Mix (Vazyme, Q311) on the CFX Connect Thermal Cycler (BIO-RAD). The fold changes of the target genes relative to the control cells were calculated using the ΔΔCt method, with normalization to GAPDH expression. Please refer to Supplementary Data 4 for a list of all qPCR primers used.

Chromatin immunoprecipitation (ChIP)

ChIP experiments were carried out according to the standard protocol provided by the SimpleChIP Plus Sonication Chromatin IP Kit (CST, 56383). HEK293R cells were transfected with Flag-tagged dCas9 activators together with gTetO. Sonication was performed using the Bioruptor pico (Diagenode) by applying 10 cycles of 30 s ON and 30 s OFF to obtain chromatin fragments of ~100–500 bp. The anti-Flag antibody (Proteintech, 20543-1-AP), anti-BRG1 antibody (Abcam, ab110641), anti-RNA Polymerase II RPB1 antibody (BioLegend, 664906), anti-MED1 antibody (Abcam, ab64965) and Normal Rabbit IgG (Cell Signaling, 2729S) were used. ChIP DNA was purified using the Zymo ChIP DNA cleanup kit (Zymo, D5205). The ChIP enrichment was analyzed by quantitative PCR.

Co-immunoprecipitation (co-IP) and western blotting (WB)

HEK293T cells transfected with Flag-tagged dCas9 activators along with gRNAs targeting NTF3 or IL1RN promoter were harvested and homogenized in lysis buffer (20 mM Tris-HCl pH 7.4, 150 mM NaCl, 1 mM EDTA, 1% Triton X-100, protease inhibitor cocktail (TargetMol, C0001) with 2 h of rotation. Following centrifugation, the protein lysates in the supernatant were collected, and their concentrations were determined using the BCA Protein Quantification Kit (Vazyme, E112-01). For immunoprecipitation, the protein lysates were incubated overnight with rotation using an anti-Flag antibody (Proteintech, 20543-1-AP) and Normal Rabbit IgG (Cell Signaling, 2729S). Subsequently, ChIP-Grade Protein G Magnetic Beads (Cell Signaling, 9006S) were introduced to each reaction. After an additional 2 h of rotation, the beads were washed four times with lysis buffer and eluted by heating at 95 °C for 10 min. The eluted proteins were loaded onto an 8% PAGE gel for separation and transferred to PVDF membranes using wet/tank blotting systems. Afterwards, the PVDF membranes were blocked using 5% skim milk powder/TBST and then incubated overnight at 4 °C with primary antibodies, including anti-Flag antibody (Proteintech, 20543-1-AP), anti-BRG1 antibody (Abcam, ab110641), anti-RNA Polymerase II RPB1 antibody (BioLegend, 664906), and anti-MED1 antibody (Abcam, ab64965). Following three washes with TBST, the membranes were incubated with secondary antibodies for 1 h at room temperature. Subsequently, the membranes were washed three times with TBST and incubated with Clarity Western ECL substrate (Bio-Rad, 170-5061). The protein bands were detected using a ChemiDoc XRS+ imaging system (Bio-Rad).

mRNA-seq library construction and data processing

RNA was isolated from HEK293R cells transfected with dCas9-VP64 or dCas9-VP64-FUS, along with gTetO and gScr, using the TRIzol™ reagent (Invitrogen, 15596018). Subsequently, mRNA-seq libraries were prepared using the Hieff NGS® Ultima Dual-mode mRNA Library Prep Kit (Yeasen, 12309), with 2 μg of total RNA input. Briefly, mRNA was captured and purified from the total RNA using oligo(dT) RNA capture beads. Following fragmentation, strand-specific ds-cDNAs were synthesized through a two-step linear amplification process and ligated to sequencing adapters. The cDNA fragments, ranging from 350 to 450 bp, were selected and purified using the Hieff NGS® DNA Selection Beads (Yeasen, 12601). Finally, libraries were amplified with indexed primers for 12 cycles of PCR and sequenced on the NovaSeq 6000 platform (Illumina) in a 2 × 150 nt manner.

For mRNA-seq data analysis, clean reads were aligned to human reference genome (hg38) supplemented with GFP sequence by HISAT2[66]. Aligned reads were inputted into featureCounts[67] for counting the read number of coding genes and GFP. The genome annotation gtf file was obtained from Ensemble v105 and only coding genes and additional GFP annotation were used for count. The differential expression genes were identified using DEseq2[68].

Statistics and reproducibility

All experiments were independently repeated at least three times with consistent results. The number of replicates in each experiment is indicated in the figure legends and/or methods. Bar plot data are expressed as means ± SD using Prism software (GraphPad). Statistical comparisons were performed using one-way ANOVA followed by Welch's test or a two-sided Welch's t-test. Boxplot data are presented as the median fluorescence intensity, with the 25th and 75th quartiles, as well as the 5th and 95th percentiles. Statistical significance was determined by a two-sided Wilcoxon rank-sum test. A P-value of <0.05 was considered statistically significant.

Reporting summary

Further information on research design is available in the Nature Portfolio Reporting Summary linked to this article.

Data availability

The RNA-seq data generated from this study have been submitted to the NCBI under the accession number GSE248523. All materials, protocols and described in this study are available from the corresponding author upon request. Source data are provided with this paper.

References

1. Soto, L. F. et al. Compendium of human transcription factor effector domains. *Mol. Cell* **82**, 514–526 (2022).
2. Lambert, S. A. et al. The human transcription factors. *Cell* **175**, 598–599 (2018).
3. Lee, T. I. & Young, R. A. Transcriptional regulation and its misregulation in disease. *Cell* **152**, 1237–1251 (2013).
4. Hafner, A. & Boettiger, A. The spatial organization of transcriptional control. *Nat. Rev. Genet.* **24**, 53–68 (2023).
5. Beerli, R. R. & Barbas, C. F. 3rd Engineering polydactyl zinc-finger transcription factors. *Nat. Biotechnol.* **20**, 135–141 (2002).
6. Beerli, R. R., Dreier, B. & Barbas, C. F. 3rd. Positive and negative regulation of endogenous genes by designed transcription factors. *Proc. Natl Acad. Sci. USA* **97**, 1495–1500 (2000).
7. Maeder, M. L. et al. Robust, synergistic regulation of human gene expression using TALE activators. *Nat. Methods* **10**, 243–245 (2013).
8. Perez-Pinera, P. et al. Synergistic and tunable human gene activation by combinations of synthetic transcription factors. *Nat. Methods* **10**, 239–242 (2013).
9. Zhang, F. et al. Efficient construction of sequence-specific TAL effectors for modulating mammalian transcription. *Nat. Biotechnol.* **29**, 149–153 (2011).
10. Gilbert, L. A. et al. CRISPR-mediated modular RNA-guided regulation of transcription in eukaryotes. *Cell* **154**, 442–451 (2013).
11. Maeder, M. L. et al. CRISPR RNA-guided activation of endogenous human genes. *Nat. Methods* **10**, 977–979 (2013).
12. Perez-Pinera, P. et al. RNA-guided gene activation by CRISPR-Cas9-based transcription factors. *Nat. Methods* **10**, 973–976 (2013).

13. Dominguez, A. A., Lim, W. A. & Qi, L. S. Beyond editing: repurposing CRISPR-Cas9 for precision genome regulation and interrogation. *Nat. Rev. Mol. Cell Biol.* **17**, 5–15 (2016).
14. Chavez, A. et al. Comparison of Cas9 activators in multiple species. *Nat. Methods* **13**, 563–567 (2016).
15. Chavez, A. et al. Highly efficient Cas9-mediated transcriptional programming. *Nat. Methods* **12**, 326–328 (2015).
16. Tanenbaum, M. E., Gilbert, L. A., Qi, L. S., Weissman, J. S. & Vale, R. D. A protein-tagging system for signal amplification in gene expression and fluorescence imaging. *Cell* **159**, 635–646 (2014).
17. Konermann, S. et al. Genome-scale transcriptional activation by an engineered CRISPR-Cas9 complex. *Nature* **517**, 583–588 (2015).
18. Liao, H. K. et al. In vivo target gene activation via CRISPR/Cas9-mediated trans-epigenetic modulation. *Cell* **171**, 1495–1507.e1415 (2017).
19. Zhou, H. et al. In vivo simultaneous transcriptional activation of multiple genes in the brain using CRISPR-dCas9-activator transgenic mice. *Nat. Neurosci.* **21**, 440–446 (2018).
20. Banani, S. F., Lee, H. O., Hyman, A. A. & Rosen, M. K. Biomolecular condensates: organizers of cellular biochemistry. *Nat. Rev. Mol. Cell Biol.* **18**, 285–298 (2017).
21. Boija, A. et al. Transcription factors activate genes through the phase-separation capacity of their activation domains. *Cell* **175**, 1842–1855.e1816 (2018).
22. Cho, W. K. et al. Mediator and RNA polymerase II clusters associate in transcription-dependent condensates. *Science* **361**, 412–415 (2018).
23. Sabari, B. R. et al. Coactivator condensation at super-enhancers links phase separation and gene control. *Science* https://doi.org/10.1126/science.aar3958 (2018).
24. Schneider, N. et al. Liquid-liquid phase separation of light-inducible transcription factors increases transcription activation in mammalian cells and mice. *Sci. Adv.* https://doi.org/10.1126/sciadv.abd3568 (2021).
25. Liu, J. et al. CRISPR-assisted transcription activation by phase separation proteins. *Protein Cell*, https://doi.org/10.1093/procel/pwad013 (2023).
26. Chong, S. et al. Tuning levels of low-complexity domain interactions to modulate endogenous oncogenic transcription. *Mol. Cell* **82**, 2084–2097.e2085 (2022).
27. Trojanowski, J. et al. Transcription activation is enhanced by multivalent interactions independent of phase separation. *Mol. Cell* **82**, 1878–1893.e1810 (2022).
28. Xiang, S. et al. The LC domain of hnRNPA2 adopts similar conformations in hydrogel polymers, liquid-like droplets, and nuclei. *Cell* **163**, 829–839 (2015).
29. Wei, M. T. et al. Nucleated transcriptional condensates amplify gene expression. *Nat. Cell Biol.* **22**, 1187–1196 (2020).
30. Tziortzouda, P., Van Den Bosch, L. & Hirth, F. Triad of TDP43 control in neurodegeneration: autoregulation, localization and aggregation. *Nat. Rev. Neurosci.* **22**, 197–208 (2021).
31. Lu, H. et al. Phase-separation mechanism for C-terminal hyperphosphorylation of RNA polymerase II. *Nature* **558**, 318–323 (2018).
32. Liang, M. et al. Oligomerized liprin-alpha promotes phase separation of ELKS for compartmentalization of presynaptic active zone proteins. *Cell Rep.* **36**, 109476 (2021).
33. Gao, Y. et al. Multivalent m(6)A motifs promote phase separation of YTHDF proteins. *Cell Res.* **29**, 767–769 (2019).
34. Fu, Y. & Zhuang, X. m(6)A-binding YTHDF proteins promote stress granule formation. *Nat. Chem. Biol.* **16**, 955–963 (2020).
35. Celetti, G. et al. The liquid state of FG-nucleoporins mimics permeability barrier properties of nuclear pore complexes. *J. Cell Biol.* https://doi.org/10.1083/jcb.201907157 (2020).
36. Ambadipudi, S., Biernat, J., Riedel, D., Mandelkow, E. & Zweckstetter, M. Liquid-liquid phase separation of the microtubule-binding repeats of the Alzheimer-related protein Tau. *Nat. Commun.* **8**, 275 (2017).
37. Chen, Y. et al. Repurposing type I-F CRISPR-Cas system as a transcriptional activation tool in human cells. *Nat. Commun.* **11**, 3136 (2020).
38. Bracha, D. et al. Mapping local and global liquid phase behavior in living cells using photo-oligomerizable seeds. *Cell* **175**, 1467–1480.e1413 (2018).
39. Liu, Z. et al. Par complex cluster formation mediated by phase separation. *Nat. Commun.* **11**, 2266 (2020).
40. Zeng, M. et al. Reconstituted postsynaptic density as a molecular platform for understanding synapse formation and plasticity. *Cell* **174**, 1172–1187.e1116 (2018).
41. Shen, Z. et al. Biological condensates form percolated networks with molecular motion properties distinctly different from dilute solutions. *Elife*, https://doi.org/10.7554/eLife.81907 (2023).
42. Baron, M. K. et al. An architectural framework that may lie at the core of the postsynaptic density. *Science* **311**, 531–535 (2006).
43. Zhang, Q. et al. Visualizing dynamics of cell signaling in vivo with a phase separation-based kinase reporter. *Mol. Cell* **69**, 334–346.e334 (2018).
44. Carter, D., Chakalova, L., Osborne, C. S., Dai, Y. F. & Fraser, P. Long-range chromatin regulatory interactions in vivo. *Nat. Genet* **32**, 623–626 (2002).
45. Morgan, S. L. et al. Manipulation of nuclear architecture through CRISPR-mediated chromosomal looping. *Nat. Commun.* **8**, 15993 (2017).
46. Wagh, K., Garcia, D. A. & Upadhyaya, A. Phase separation in transcription factor dynamics and chromatin organization. *Curr. Opin. Struct. Biol.* **71**, 148–155 (2021).
47. Moses, D., Ginell, G. M., Holehouse, A. S. & Sukenik, S. Intrinsically disordered regions are poised to act as sensors of cellular chemistry. *Trends Biochem. Sci.* **48**, 1019–1034 (2023).
48. Lyons, H. et al. Functional partitioning of transcriptional regulators by patterned charge blocks. *Cell* **186**, 327–345.e328 (2023).
49. Linden, M. et al. FET family fusion oncoproteins target the SWI/SNF chromatin remodeling complex. *EMBO Rep.* https://doi.org/10.15252/embr.201845766 (2019).
50. Kim, Y. J. et al. Light-activated macromolecular phase separation modulates transcription by reconfiguring chromatin interactions. *Sci. Adv.* **9**, eadg1123 (2023).
51. Lee, J. H. et al. Enhancer RNA m6A methylation facilitates transcriptional condensate formation and gene activation. *Mol. Cell* **81**, 3368–3385.e3369 (2021).
52. van der Lee, R. et al. Classification of intrinsically disordered regions and proteins. *Chem. Rev.* **114**, 6589–6631 (2014).
53. Kato, M. et al. Cell-free formation of RNA granules: low complexity sequence domains form dynamic fibers within hydrogels. *Cell* **149**, 753–767 (2012).
54. Wright, P. E. & Dyson, H. J. Intrinsically disordered proteins in cellular signalling and regulation. *Nat. Rev. Mol. Cell Biol.* **16**, 18–29 (2015).
55. Lafontaine, D. L. J., Riback, J. A., Bascetin, R. & Brangwynne, C. P. The nucleolus as a multiphase liquid condensate. *Nat. Rev. Mol. Cell Biol.* **22**, 165–182 (2021).
56. Ma, S. et al. Phase-separated DropCRISPRa platform for efficient gene activation in mammalian cells and mice. *Nucleic Acids Res.* **51**, 5271–5284 (2023).
57. Wan, Y. et al. Dynamic imaging of nascent RNA reveals general principles of transcription dynamics and stochastic splice site selection. *Cell* **184**, 2878–2895.e2820 (2021).
58. Donovan, B. T., Chen, H., Jipa, C., Bai, L. & Poirier, M. G. Dissociation rate compensation mechanism for budding yeast pioneer transcription factors. *Elife* https://doi.org/10.7554/eLife.43008 (2019).
59. Wu, J. et al. Modulating gene regulation function by chemically controlled transcription factor clustering. *Nat. Commun.* **13**, 2663 (2022).

60. Klann, T. S. et al. CRISPR-Cas9 epigenome editing enables high-throughput screening for functional regulatory elements in the human genome. *Nat. Biotechnol.* **35**, 561–568 (2017).
61. Li, K. et al. Interrogation of enhancer function by enhancer-targeting CRISPR epigenetic editing. *Nat. Commun.* **11**, 485 (2020).
62. Hilton, I. B. et al. Epigenome editing by a CRISPR-Cas9-based acetyltransferase activates genes from promoters and enhancers. *Nat. Biotechnol.* **33**, 510–517 (2015).
63. Ahn, J. H. et al. Phase separation drives aberrant chromatin looping and cancer development. *Nature* **595**, 591–595 (2021).
64. Wang, J. et al. Phase separation of OCT4 controls TAD reorganization to promote cell fate transitions. *Cell Stem Cell* **28**, 1868–1883.e1811 (2021).
65. Ke, M. et al. Integrated and quantitative proteomic approach for charting temporal and endogenous protein complexes. *Anal. Chem.* **90**, 12574–12583 (2018).
66. Kim, D., Langmead, B. & Salzberg, S. L. HISAT: a fast spliced aligner with low memory requirements. *Nat. Methods* **12**, 357–360 (2015).
67. Liao, Y., Smyth, G. K. & Shi, W. featureCounts: an efficient general purpose program for assigning sequence reads to genomic features. *Bioinformatics* **30**, 923–930 (2014).
68. Love, M. I., Huber, W. & Anders, S. Moderated estimation of fold change and dispersion for RNA-seq data with DESeq2. *Genome Biol.* **15**, 550 (2014).

Acknowledgements

This work was supported by the National Key R&D Program of China (Grant No. 2021YFF1201000 and 2022YFC3400400 to W.C.), the Shenzhen Science and Technology Program (Grant No. KQTD20180411143432337 to W.C.) and the Shenzhen Key Laboratory of Gene Regulation and Systems Biology (Grant No. ZDSYS20200811144002008 to W.C.). We thank Dr. Zhou Songyang (SYSU) for providing the GFP reporter cells, Dr. Guanhua Bai (SUSTech) for the technical support, Dr. Lin Deng (SZBL), Dr. Yang Yu (IBP), and Dr. Cong Yu (SUSTech) for sharing plasmids. We also thank Dr. Mingjie Zhang (SUSTech) for helpful discussion on the project and review of the manuscript. We further thank the Center for Computational Science and Engineering of SUSTech for the support on computational resource.

Author contributions

W.C. and H.C. conceived the study. W.C., H.C., and R.C. designed the experiments. R.C., X.S., X.Y., T.G., G.H., D.N., Z.C., Y.X., and W.L. performed experiments. R.C. and S.Z.T. analyzed the NGS data. W.C., H.C., and R.C. wrote the manuscript. Y.H., M.Z., L.F., and Q.Z. discussed the results and revised the manuscript. W.C. and H.C. coordinated and supervised the study.

Competing interests

R.C., X.S., H.C., and W.C. have submitted a patent application related to this work to the China National Intellectual Property Administration (application number 202210903472.2). The remaining authors declare no competing interests.

Additional information

Supplementary information The online version contains supplementary material available at https://doi.org/10.1038/s41467-024-51694-y.

Correspondence and requests for materials should be addressed to Huanhuan Cui or Wei Chen.

Peer review information *Nature Communications* thanks the anonymous reviewers for their contribution to the peer review of this work. A peer review file is available.